PAPER

CrossMark
← click for updates

Nanoparticles of Cu_2ZnSnS_4 as performance enhancing additives for organic field-effect transistors†

Punarja Kevin,[a] Mohammad Azad Malik,[b] Paul O'Brien,[ab] Joseph Cameron,[c] Rupert G. D. Taylor,[c] Neil J. Findlay,[c] Anto R. Inigo[c] and Peter J. Skabara*[c]

The addition of oleylamine coated Cu_2ZnSnS_4 (CZTS) nanoparticles to solutions of an organic semiconductor used to fabricate organic field-effect transistors (OFETs) has been investigated. The oligothiophene-based small molecule 5T-TTF and the polymer poly(3-hexylthiophene) (P3HT) were each applied in the transistors with various concentrations of CZTS (5–20%). Atomic force microscopy (AFM) was applied to characterise the surface morphology of the OFETs. The use of 5 and 10 wt% of the CZTS nanoparticles in 5T-TTF and P3HT solutions, respectively, appears to be a simple and effective way of improving OFET performance.

Introduction

Organic semiconductors are low cost materials for organic electronic devices, such as organic field-effect transistors (OFETs), which utilise small molecules[1–3] or polymers[4–6] to achieve high charge carrier mobilities in excess of 40 cm^2 V^{-1} s^{-1}.[7] However, attempts have been made to improve the charge carrier mobility of OFETs by providing more effective pathways for charge transport by using materials such as graphene,[8,9] which acts as an electrically conducting bridge between domains in composites comprising of mainly P3HT. This led to an increased mobility with increase in the composition of graphene, showing highly stable transfer characteristics, a highest hole mobility of 1.82 cm^2 V^{-1} s^{-1} and a moderately high I_{ON}/I_{OFF} ratio of 10^4.[9] Similarly, carbon nanotubes (CNTs)[10–12] have been used in OFETs and have produced a 60-fold increase in the effective mobility of the starting semiconducting material with a minor decrease of the I_{ON}/I_{OFF} current ratio.[12] In a separate study, the addition of CNTs at a concentration of up to 10 wt%, led to a 10-fold improvement in field-effect mobility in P3HT OFETs.[11] The use of inorganic nanomaterials in OFET devices is under-explored and yet there is a vast array of such materials with broadly varying properties to choose from. Kesterites such as Cu_2ZnSnS_4 (CZTS) have attracted considerable recent interest[13–17] because

they are composed of elements that are earth abundant, of low toxicity and hence relatively environmentally benign. In addition to their good absorption characteristics, such as broad absorption spectra and tunable band gaps, kesterite nanoparticles exhibit good charge transport and have been used in devices such as FETs with good performance.[15,18] These materials are therefore exciting potential additives for improving the transistor characteristics of organic semiconductors in OFETs, as well as in organic solar cells and organic layers (hole and electron transport layers) of perovskite solar cells.

In this work we demonstrate that oleylamine coated CZTS nanoparticles, used in low concentration, can be used as an additive in organic semiconductor solutions for the enhancement of charge carrier mobility in OFET devices. Often nanoparticles are processed in a ligand-exchange solution, with the long ligands of the nanoparticles exchanged for shorter ligands such as butylamine,[19] ethanedithiol[20] or benzenedithiol[21] in order to reduce the distance between particles. However, in this study we show that the kesterite nanoparticles capped with long ligands can be used to improve the performance of transistor devices. The simple addition of these nanoparticles to organic semi-conductor solutions reduces the need for complex processing techniques or toxic ligands normally required.

Synthesis of CZTS nanoparticles

The compounds $[Cu(S_2CNEt_2)_2]$ (**1**), $[Zn(S_2CNEt_2)_2]$ (**2**) and $[^nBu_2Sn(S_2CNEt_2)_2]$ (**3**) were synthesised as reported in the literature.[22–25] The CZTS nanocrystals were synthesised, under dry nitrogen atmosphere, using a Schlenk line by a modification of a published procedure.[27] In a typical synthesis, 20 ml oleylamine was heated to 90 °C and purged under N$_2$. The complexes were used as follows: 1.0 g (2.8 mmol) of $[Cu(S_2CNEt_2)_2]$, 0.50 g (1.4 mmol) of

[a] *School of Chemistry, The University of Manchester, M13 9PL, UK*
[b] *School of Materials, The University of Manchester, M13 9PL, UK*
[c] *WestCHEM, Department of Pure and Applied Chemistry, University of Strathclyde, G1 1XL, UK. E-mail: peter.skabara@strath.ac.uk*

† Electronic supplementary information (ESI) available: p-XRD data for CZTS grown under different temperatures (180 °C, 220 °C and 250 °C); OFET data for transistors fabricated with oleylamine only as the additive; TGA analyses of samples **1**–**3**. See DOI: 10.1039/c6tc01650b

This journal is © The Royal Society of Chemistry 2016

J. Mater. Chem. C, 2016, **4**, 5109–5115 | 5109

[Zn(S₂CNEt₂)₂] and 0.73 g (1.4 mmol) of [$^nBu_2Sn(S_2CNEt_2)_2$] were mixed and ground in a mortar and pestle, and then added to the hot degassed oleylamine. The temperature of the solution was then raised to the processing temperature: 180, 220 or 250 °C. This temperature was maintained for 1 hour. The nanocrystals were precipitated by dispersing in methanol and were centrifuged for 5–10 min at 4000 rpm. The supernatant was discarded and the nanocrystals were redispersed in hexane. The precipitation and dispersion steps were repeated several times to remove excess oleylamine. Finally, the nanocrystals were stored for later use by dispersing in hexane or dried and kept under N₂. The nanoparticles appear to be stable for more than six months.

Nanoparticle characterisation

The nanoparticles were characterised using p-XRD, TEM, HRTEM, UV-vis absorption spectroscopy and photoluminescence spectroscopy. The X-ray diffraction (XRD) studies were performed on a Bruker AXSD8 diffractometer using CuKα radiation. The samples were mounted flat and scanned between 20° and 80° in a step size of 0.05°. Nanoparticles in hexane were deposited on 400 mesh copper Formvar/carbon grids for TEM work. TEM images were collected on a Technai T20 microscope using an accelerating voltage of 300 kV. STEM imaging and energy dispersive X-ray (EDX) spectrum imaging were performed using a probe side aberration corrected Titan ChemiSTEM instrument operated at 200 kV with a probe current of ~440 pA. The nanoscale elemental map images were analysed using Aztec software. TEM images were analysed by Gatan Digital Micrograph software. The XPS spectra were collected using a Kratos Axis Ultra in the School of Materials in the University of Manchester.

OFET fabrication

Organic field-effect transistors were fabricated on SiO₂ substrates with prefabricated interdigitated Au source-drain channels with lengths of 2.5, 5, 10 and 20 μm and width of 1 cm. N-doped Si and SiO₂ were the gate electrode and gate dielectric materials, respectively. The substrates were cleaned using water, acetone and ethanol before being treated in UV-ozone for 30 seconds. A pentafluorobenzenethiol (PFBT) self-assembled monolayer (SAM) was prepared by drop-casting a solution of PFBT (10 mM in ethanol) onto the substrate. After 1 min, the residual PFBT was then washed away with ethanol and the substrate was dried over a stream of compressed air. Similarly, an octadecyltrichlorosilane (OTS) SAM was prepared by drop-casting an OTS solution (13 mM in toluene) onto the substrate which was washed with toluene and dried after 1 minute.

The conditions for the fabrication of OFETs using 4,4′,6,6′-tetrakis(3′-hexyl-5′-methyl-[2,2′-bithiophen]-5-yl)-2,2′-bithieno[3,4-d]-[1,3]dithiolylidene (5T-TTF) were the same as those previously reported[26] with the addition of differing amounts of CZTS as the only variable. All OFETs fabricated using P3HT were made using PFBT and OTS SAMs by spin-coating a 5 mg ml⁻¹ solution of the polymer at 2000 rpm with varying amounts of CZTS onto the substrate and annealing at 150 °C. Every OFET fabricated was spin-coated from a solution which had been subjected to ultra-sonication for 20 minutes.

Current–voltage characteristics were recorded using a Keithley 4200 semiconductor characterisation system at room temperature in a nitrogen filled glove box where oxygen and water levels were maintained below 0.1 ppm. The field-effect mobilities were determined from the saturation regime and calculated using the following equation:

$$\mu_{sat} = \frac{2L}{WC_i} \times \left(\frac{\partial\sqrt{I_{DS}}}{\partial V_{GS}}\right)^2$$

where I_{DS} is the drain current, μ_{sat} is the saturation carrier mobility, V_{GS} is the gate voltage, L is the channel length, W is the channel width and C_i is the capacitance per unit area of the insulator material. The mobility values reported were calculated from the average mobility of six devices and the standard deviation (σ) is shown for the OFETs fabricated. The surface morphologies of the OFETs were characterised using a Dimension 3100 atomic force microscope (AFM) in tapping mode.

Results and discussion

CZTS nanoparticles

The synthesis of CZTS nanoparticles was previously carried out using a mixture of [Cu(S₂CNEt₂)₂] (1), [Zn(S₂CNEt₂)₂] (2) and [Sn(S₂CNEt₂)₄] (4) in octadecene and oleic acid, followed by injection into oleylamine.[27] Herein we report a method using [$^nBu_2Sn(S_2CNEt_2)_2$] (3) in place of [Sn(S₂CNEt₂)₄] (4) in oleylamine. The reported decomposition temperatures of copper, zinc and tin diethyldithiocarbamates (1), (2) and (4)[27] are 220 °C (1), 240 °C (2), and 174 °C (4),[18,24,27] which may have led to premature decomposition/over-incorporation of tin due to the lower decomposition temperature of the [Sn(S₂CNEt₂)₄]. In our studies, thermogravimetric analysis (TGA) of the complexes (1), (2) and (3) (Fig. S3, ESI†), showed more compatible and sharp
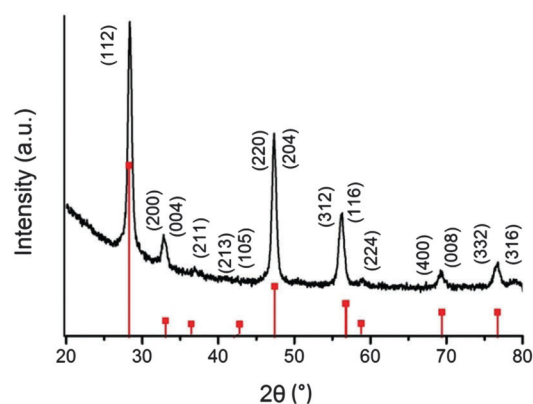

Fig. 1 The p-XRD patterns of CZTS nanoparticles synthesised at 220 °C for 1 hour. The reference patterns are of kesterite CZTS (ICDD: 04-015-0223). The TEM images showed hexagonal particles with an average size of 10 ± 2 nm. The high resolution TEM (HRTEM) images shown in Fig. 2a and b, exhibit clear lattice fringes with measured d-spacing of ca. 0.313(1) nm corresponding to the (112) lattice plane of the kesteritic CZTS structure (Fig. 2c). The elemental composition of the CZTS nanocrystals was determined by energy dispersive X-ray spectroscopy (EDX), which gave a Cu/Zn/Sn/S composition (atomic%) of Cu (28.43%), Zn (11.38%), Sn (12.85%) and S (47.34%).

decomposition starting at 284 °C (**1**), 303 °C (**2**) and 300 °C (**3**), all leading to their corresponding metal sulphides. The mid-point of each decomposition is within 5 °C of 330 °C. These TGA results for complexes (**1**), (**2**) and (**3**) match well with our previous reports.[28] The difference in the decomposition temperatures between this work and earlier reports may be due to the method of reporting or experimental differences.

The p-XRD pattern (Fig. 1) of the sample prepared at 220 °C for 1 hour shows main peaks at d-spacings of: 3.14, 2.73, 1.92, 1.64, 1.35, 69.34 and 1.24 for the (112), (200), (204), (312), (400) and (316) spacings of kesterite CZTS (ICDD: 04-015-0223).[24] The p-XRD patterns of samples formed at other temperatures are shown in the ESI† (Fig. S1).

The stoichiometry of the material is $Cu_{2.5}Zn_1Sn_{1.1}S_4$, which is slightly Cu rich (however Cu grids were used for the TEM). Fig. 2d shows the selected area elemental map for the nanoparticles synthesised at 220 °C; it shows a uniform distribution of the elements in the entire area of analysis.
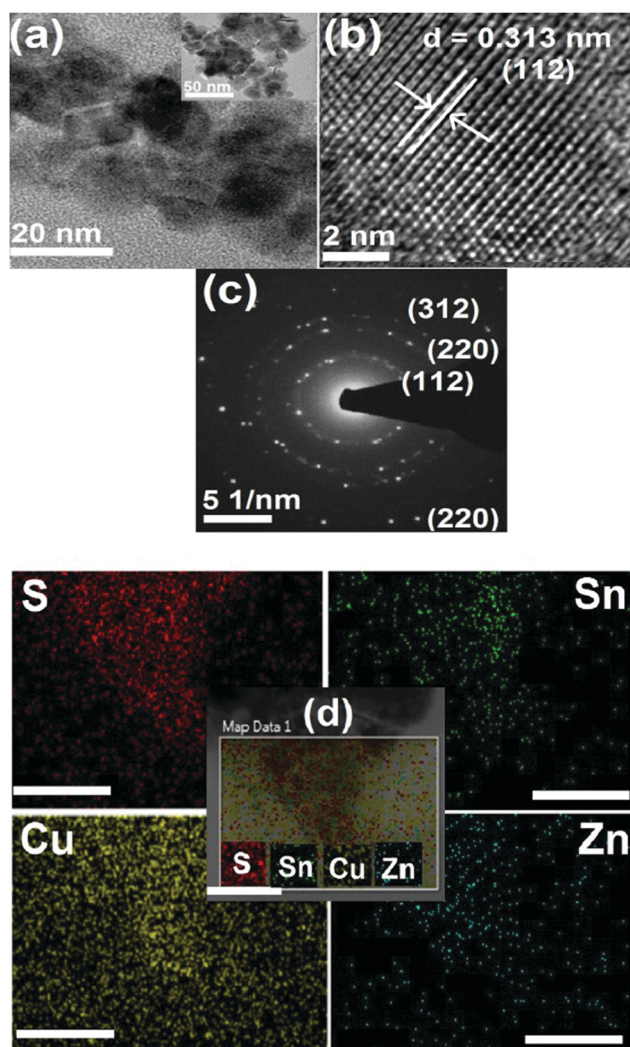

Fig. 2 (a) and (b) are the HRTEM images, (c) the diffraction patterns and (d) the elemental map of CZTS nanoparticles synthesised at 220 °C. The scale bar shown for the elemental map is *ca.* 50 nm.
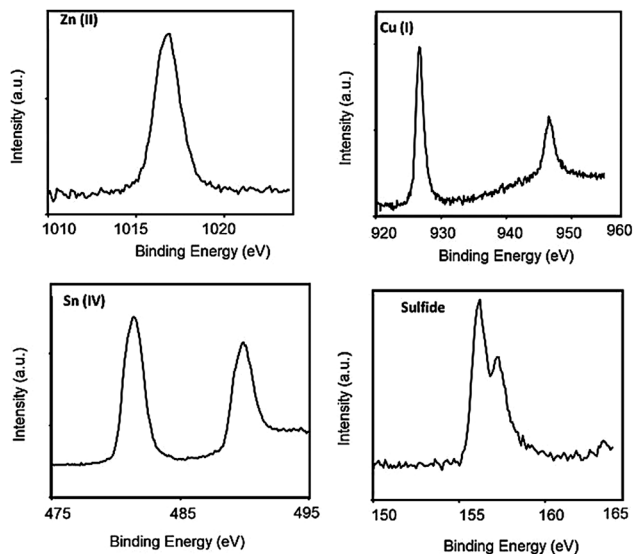

Fig. 3 High resolution XPS spectra of CZTS nanoparticles synthesised at 220 °C.

The valence state of the elements in the nanoparticles synthesised at 220 °C were determined by XPS (Fig. 3); binding energies were as follows: Zn $2p_{3/2}$, 1017 eV; Cu $2p_{3/2}$, 926 eV; Cu $2p_{1/2}$, 947 eV; Sn $3d_{5/2}$, 480 eV; Sn $3d_{3/2}$, 491 eV; S $2p_{3/2}$, 156 eV; S $2p_{1/2}$ 158 eV. The values are commensurate with the valence states Cu(I), Sn(IV), Zn(I) and S^{2-}.[25]

Organic field-effect transistors

The details of OFET fabrication using both 5T-TTF and P3HT organic semiconductors are given in the experimental section. The results for OFETs fabricated using 5T-TTF are summarised below in Table 1. OFETs fabricated using only 5T-TTF show an average hole mobility of 9.5×10^{-3} cm^2 V^{-1} s^{-1}, which is similar to that determined previously.[26] The output and transfer characteristics for the devices tested are shown below in Fig. 4a and b. The current response is increased (Fig. 4c) for the OFET fabricated using 5 wt% CZTS and the hole mobility calculated is 0.016 cm^2 V^{-1} s^{-1}, a 68% increase with respect to the device fabricated using pristine 5T-TTF. The I_{ON}/I_{OFF} ratio remains the same for both devices. When the nanoparticle concentration is increased, there is no saturation observed in the output graph. In order to investigate the OFET performance further, AFM was used in tapping mode to characterise the surface morphology of the different devices; these images are

Table 1 Data for OFETs fabricated from 5T-TTF with various concentrations of CZTS nanoparticles

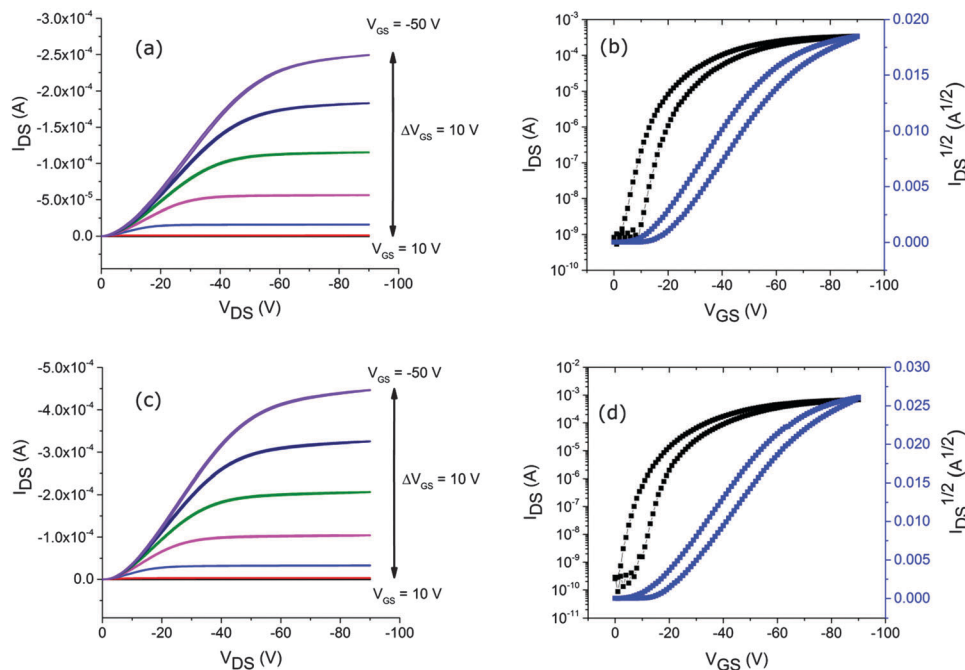| Compound	V_{Th} (V)	ON/OFF ratio	Average μ_{hole} (cm^2 V^{-1} s^{-1})	$\sigma\mu_{hole}$
5T-TTF	−13	10^3	9.5×10^{-3}	5.8×10^{-3}
5T-TTF + 1% CZTS	−17	10^3	8.5×10^{-3}	3.8×10^{-3}
5T-TTF + 2.5% CZTS	−17	10^3	8.3×10^{-3}	4.6×10^{-3}
5T-TTF + 5% CZTS	−15	10^3	0.016	4.6×10^{-3}
5T-TTF + 10% CZTS	—	—	—	

Fig. 4 (a) and (b) show the output and transfer characteristics for an OFET fabricated using 5T-TTF; (c) and (d) are the output and transfer characteristics for an OFET fabricated with 5T-TTF + 5% CZTS.
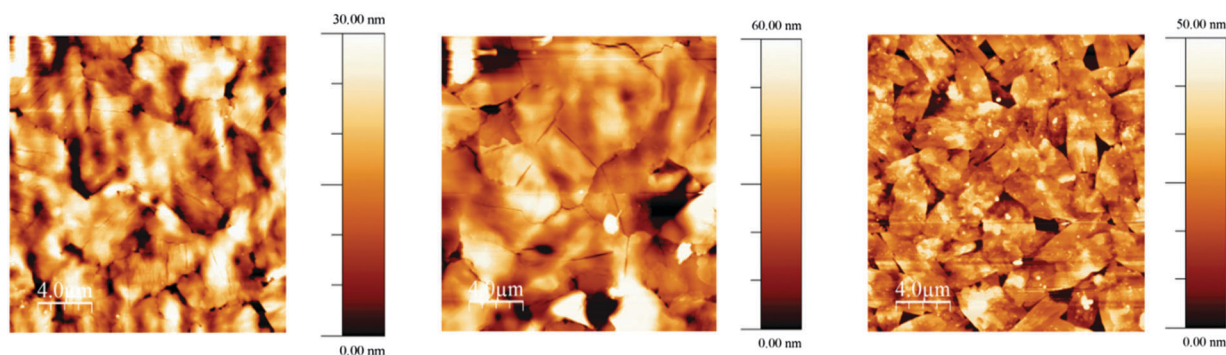

Fig. 5 AFM images of OFETs fabricated from 5T-TTF (left), 5T-TTF + 5% CZTS (centre) and 5T-TTF + 10% CZTS (right)

shown in Fig. 5. The surface of the OFET fabricated using 5T-TTF is comparable to the image of the surface from the previously fabricated device.[26] Surprisingly, despite the increased roughness of the surface of the device fabricated with 5 wt% CZTS, compared to the pristine organic film, the hole mobility is higher. As the concentration of CZTS is increased to 10%, there is a significant change in morphology with the 5T-TTF domains being broken up. The emergence of a number of gaps in the film explains the poor performance for this device.

The behaviour of the OFETs fabricated using P3HT and CZTS is slightly different to those from 5T-TTF and the device data for each OFET are summarised in Table 2. The output and transfer characteristics for the OFET fabricated using P3HT without any additives are shown in Fig. 6a and b. The average hole mobility calculated for P3HT is 0.041 cm^2 V^{-1} s^{-1} and in a similar trend to the 5T-TTF OFET, when 5 wt% CZTS is added to the solution used for OFET fabrication there is an increase in

Table 2 Results for fabricated OFETs from P3HT with various concentrations of CZTS

Compound	V_{Th} (V)	ON/OFF ratio	Average μ_{hole} (cm^2 V^{-1} s^{-1})	$\sigma\mu_{hole}$
P3HT	−8	10^2	0.041	0.015
P3HT + 5% CZTS	−9	10^2	0.053	0.012
P3HT + 10% CZTS	−10	10^2	0.088	0.013
P3HT + 15% CZTS	−10	10^2	0.037	9.6 × 10^{-3}
P3HT + 20% CZTS	−10	10^2	0.033	0.016

the mobility. The output and transfer graphs for this device are shown in Fig. 6c and d. The calculated hole mobility (0.053 cm^2 V^{-1} s^{-1}) is 29% higher than the OFET fabricated without any nanoparticles. However, unlike the oligomer based OFETs where 10% CZTS led to a deterioration in performance, OFETs fabricated with P3HT and 10% CZTS (Fig. 6e and f) showed a further increase in charge carrier mobility, with the

average mobility calculated as 0.088 cm^2 V^{-1} s^{-1}, a 115% increase compared to the value for the device fabricated using only the polymer. In contrast, a further increase in nanoparticle concentration to 15% or 20% shows charge carrier mobilities only slightly lower than the OFET fabricated with a neat P3HT film, showing that performance is not enhanced by the addition of higher concentrations of nanoparticles.

The AFM images for P3HT devices are shown in Fig. 7 and give a clear trend. The device fabricated using neat P3HT shows a number of polymer aggregates on the surface. As 5 wt% CZTS is added to the solution, the resulting device still shows P3HT aggregates, but overall there are fewer of these domains. There is a further reduction in the surface roughness as the CZTS concentration is increased to 10% and there appears to be a significant decrease in the size of the P3HT aggregates. The domain sizes are slightly larger when the concentration is

increased to 15% CZTS and the surface roughness also increases, but the aggregates are smaller than those present in the neat polymer film. This suggests that, although the P3HT aggregates are being broken up in films formed from 15% and 20% CZTS solutions, charge transport is inhibited by the increased nanoparticle concentration and therefore leads to a charge carrier mobility that is slightly reduced with respect to OFETs fabricated using P3HT. It is worth noting that the OFET performance does not tail off as significantly as when the CZTS concentration is increased for 5T-TTF containing OFETs.

Finally, in an attempt to determine if the nanoparticles or the oleylamine ligands are responsible for the improved performance, P3HT OFETs were fabricated using 5% v/v and 10% v/v oleylamine. The output and transfer characteristics for each of these OFETs are shown in the ESI† (Fig. S2). The addition of 5% oleylamine leads to a severely reduced mobility ($\mu_h = 2.83 \times 10^{-3}$ cm^2 V^{-1} s^{-1}) and
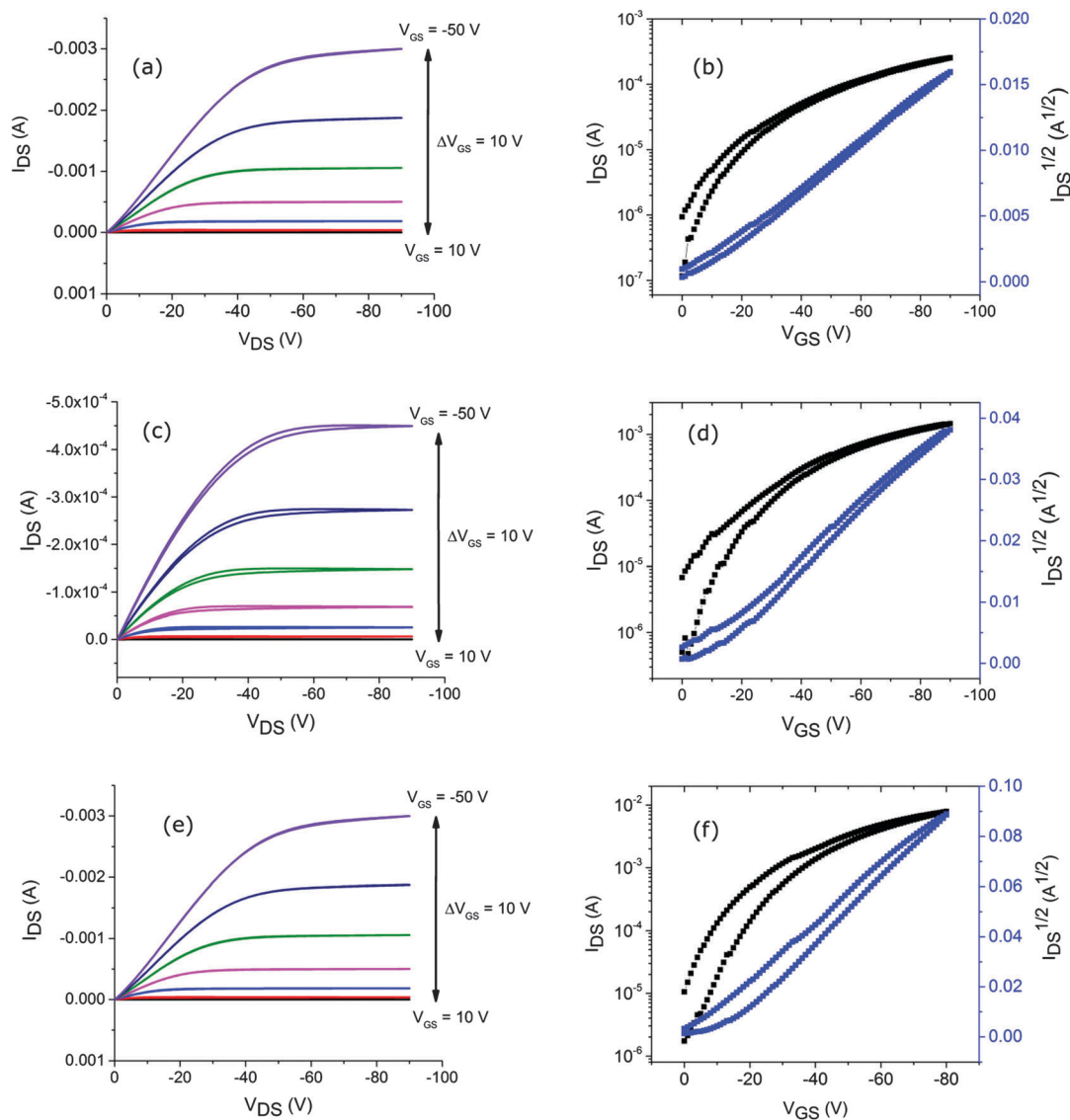

Fig. 6 Output and transfer characteristics (left and right columns, respectively), for OFETs fabricated using neat P3HT [(a) and (b)], P3HT + 5% CZTS [(c) and (d)], and P3HT + 10% CZTS [(e) and (f)].
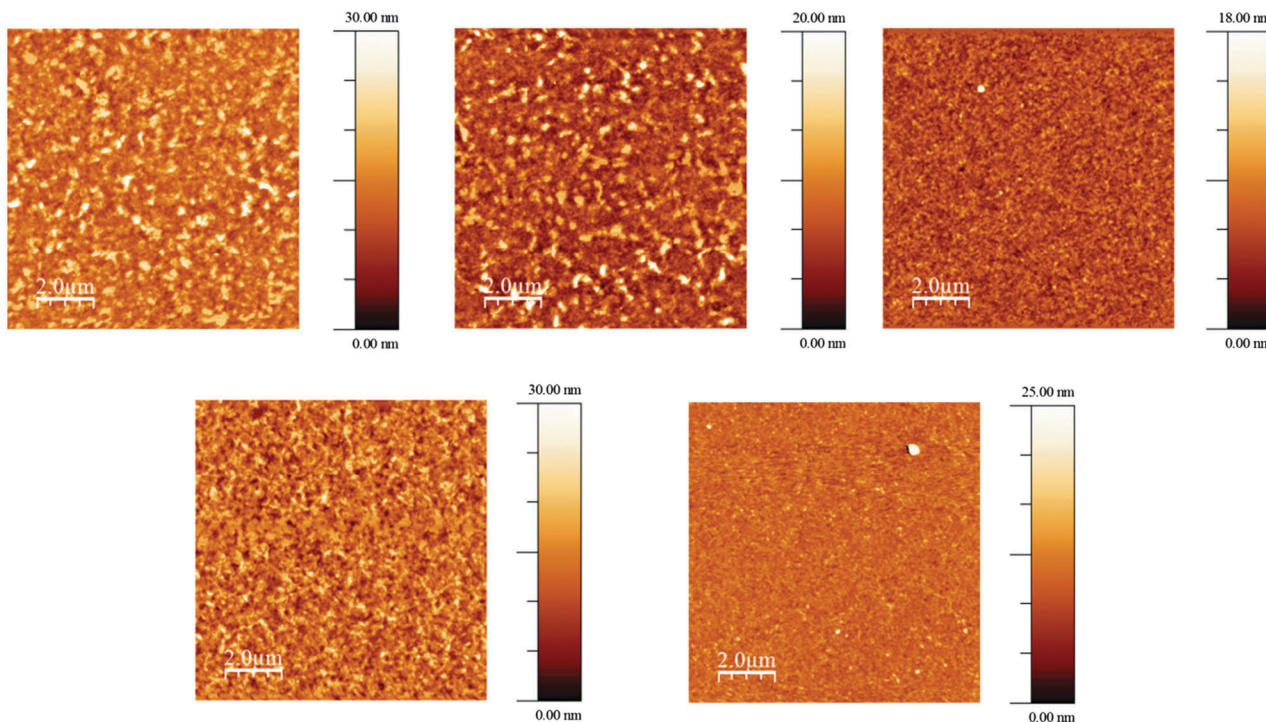
Fig. 7 AFM images for OFETs fabricated using P3HT (top, left), P3HT + 5% CZTS (top, centre), P3HT + 10% CZTS (top, right), P3HT + 15% CZTS (bottom, left) and P3HT + 20% CZTS (bottom, right).

although this is improved with 10% oleylamine ($\mu_h = 6.07 \times 10^{-3} \text{ cm}^2 \text{ V}^{-1} \text{ s}^{-1}$), the performance of both devices is considerably poorer than any of the devices fabricated using P3HT and CZTS. This would suggest that the nanoparticles are responsible for improving the OFET performance rather than the long oleylamine ligands.

Conclusion

CZTS nanoparticles have been used as additives for the fabrication of solution-processed OFETs. The nanoparticle composites (5% CZTS) with 5T-TTF had a hole mobility 68% higher than devices using only the oligomer, whilst 10% addition to P3HT devices led to a hole mobility more than double (115% increase) that of the OFET with neat P3HT. The additives are inexpensive and environmentally benign, which suggests that they have potential for the improvement of OFETs. Reports on applications of inorganic nanoparticles in OFETs are sparse in the literature and have been limited mainly to their use as nanocomposites in gate dielectric layers.[29–31] Zinc oxide nanoparticles have been used in polyfluorene composites for light-emitting field effect transistors,[32] whilst Q-ZnO has been applied as a component in a hybrid OFET bilayer device fabricated with P3HT as the organic film.[33] Blends of P3HT and CdSe have been studied in OFETs[34] and also in organic photovoltaics devices.[35] However, the mechanism of charge transport in these composites is not well understood. It has been shown by low temperature light-induced electron spin resonance studies that the morphology of P3HT changes in the presence of CdSe nanoparticles[34] and that charge transfer between the two components only takes place efficiently if

the CdSe capping ligand is removed. In OFETs, however, the structure of the capping ligand in P3HT/CdSe composites influences the value of the mobility.[35] This begs the question whether or not the inorganic nanoparticles in hybrid OFETs change the characteristics of the device as a function of morphology or if the role of the inorganic material is more complex. It is perhaps more intuitive to assume the former and our work clearly shows that morphology changes with different loadings of CZTS nanoparticles. However, an in-depth study needs to be conducted to elucidate the full role of CZTS in composites. One would expect that the inclusion of nanoparticles into pristine molecular (5T-TTF) and polymeric (P3HT) materials would disrupt long-range order and affect charge transport detrimentally, and remarkably we see an enhancement of hole mobility upon the application of CZTS nanoparticles. One possible explanation is that the inorganic material reduces the density of traps in the organic layer and this has been seen in the case of MEH-PPV/ZnO blends.[36]

Acknowledgements

5114 | *J. Mater. Chem. C*, 2016, **4**, 5109–5115

This journal is © The Royal Society of Chemistry 2016

Notes and references

1 Y. Qiao, Y. Guo, C. Yu, F. Zhang, W. Xu, Y. Liu and D. Zhu, *J. Am. Chem. Soc.*, 2012, **134**, 4084–4087.

2 R. Pfattner, M. Mas-Torrent, I. Bilotti, A. Brillante, S. Milita, F. Liscio, F. Biscarini, T. Marszalek, J. Ulanski, A. Nosal, M. Gazicki-Lipman, M. Leufgen, G. Schmidt, L. W. Molenkamp, V. Laukhin, J. Veciana and C. Rovira, *Adv. Mater.*, 2010, **22**, 4198–4203.

3 E. D. Głowacki, M. Irimia-Vladu, M. Kaltenbrunner, J. Gsiorowski, M. S. White, U. Monkowius, G. Romanazzi, G. P. Suranna, P. Mastrorilli, T. Sekitani, S. Bauer, T. Someya, L. Torsi and N. S. Sariciftci, *Adv. Mater.*, 2013, **25**, 1563–1569.

4 H.-R. Tseng, H. Phan, C. Luo, M. Wang, L. A. Perez, S. N. Patel, L. Ying, E. J. Kramer, T.-Q. Nguyen, G. C. Bazan and A. J. Heeger, *Adv. Mater.*, 2014, **26**, 2993–2998.

5 I. Meager, M. Nikolka, B. C. Schroeder, C. B. Nielsen, M. Planells, H. Bronstein, J. W. Rumer, D. I. James, R. S. Ashraf, A. Sadhanala, P. Hayoz, J.-C. Flores, H. Sirringhaus and I. McCulloch, *Adv. Funct. Mater.*, 2014, **24**, 7109–7115.

6 S. Park, B. T. Lim, B. Kim, H. J. Son and D. S. Chung, *Sci. Rep.*, 2014, **4**, 5482.

7 Y. Yuan, G. Giri, A. L. Ayzner, A. P. Zoombelt, S. C. B. Mannsfeld, J. Chen, D. Nordlund, M. F. Toney, J. Huang and Z. Bao, *Nat. Commun.*, 2014, **5**, 3005.

8 J. Huang, D. R. Hines, B. J. Jung, M. S. Bronsgeest, A. Tunnell, V. Ballarotto, H. E. Katz, M. S. Fuhrer, E. D. Williams and J. Cumings, *Org. Electron.*, 2011, **12**, 1471–1476.

9 M. El Gemayel, A. Narita, L. F. Dossel, R. S. Sundaram, A. Kiersnowski, W. Pisula, M. R. Hansen, A. C. Ferrari, E. Orgiu, X. Feng, K. Mullen and P. Samori, *Nanoscale*, 2014, **6**, 6301–6314.

10 S. Park, S. Jin, G. Jun, S. Jeon and S. Hong, *Nano Res.*, 2011, **4**, 1129–1135.

11 Y. D. Park, J. A. Lim, Y. Jang, M. Hwang, H. S. Lee, D. H. Lee, H.-J. Lee, J.-B. Baek and K. Cho, *Org. Electron.*, 2008, **9**, 317–322.

12 X.-Z. Bo, C. Y. Lee, M. S. Strano, M. Goldfinger, C. Nuckolls and G. B. Blanchet, *Appl. Phys. Lett.*, 2005, **86**, 182102.

13 P. Jackson, D. Hariskos, E. Lotter, S. Paetel, R. Wuerz, R. Menner, W. Wischmann and M. Powalla, *Prog. Photovoltaics*, 2011, **19**, 894–897.

14 W. Wang, M. T. Winkler, O. Gunawan, T. Gokmen, T. K. Todorov, Y. Zhu and D. B. Mitzi, *Adv. Energy Mater.*, 2014, **4**, 1301465.

15 W. Yang, H.-S. Duan, K. C. Cha, C.-J. Hsu, W.-C. Hsu, H. Zhou, B. Bob and Y. Yang, *J. Am. Chem. Soc.*, 2013, **135**, 6915–6920.

16 B. Shin, O. Gunawan, Y. Zhu, N. A. Bojarczuk, S. J. Chey and S. Guha, *Prog. Photovoltaics*, 2013, **21**, 72–76.

17 H. Zhou, H.-S. Duan, W. Yang, Q. Chen, C.-J. Hsu, W.-C. Hsu, C.-C. Chen and Y. Yang, *Energy Environ. Sci.*, 2014, **7**, 998–1005.

18 L. Arora, V. Singh, G. Partheepan, T. D. Senguttuvan and K. Jain, *Appl. Nanosci.*, 2015, 1–10.

19 G. Konstantatos, I. Howard, A. Fischer, S. Hoogland, J. Clifford, E. Klem, L. Levina and E. H. Sargent, *Nature*, 2006, **442**, 180–183.

20 J. M. Luther, M. Law, Q. Song, C. L. Perkins, M. C. Beard and A. J. Nozik, *ACS Nano*, 2008, **2**, 271–280.

21 G. I. Koleilat, L. Levina, H. Shukla, S. H. Myrskog, S. Hinds, A. G. Pattantyus-Abraham and E. H. Sargent, *ACS Nano*, 2008, **2**, 833–840.

22 N. Revaprasadu, M. A. Malik and P. O'Brien, *S. Afr. J. Chem.*, 2004, **57**, 40–43.

23 M. B. Hursthouse, M. A. Malik, M. Motevalli and P. O'Brien, *J. Mater. Chem.*, 1992, **2**, 949–955.

24 K. Ramasamy, V. L. Kuznetsov, K. Gopal, M. A. Malik, J. Raftery, P. P. Edwards and P. O'Brien, *Chem. Mater.*, 2013, **25**, 266–276.

25 A. V. Moholkar, S. S. Shinde, G. L. Agawane, S. H. Jo, K. Y. Rajpure, P. S. Patil, C. H. Bhosale and J. H. Kim, *J. Alloys Compd.*, 2012, **544**, 145–151.

26 I. A. Wright, N. J. Findlay, S. Arumugam, A. R. Inigo, A. L. Kanibolotsky, P. Zassowski, W. Domagala and P. J. Skabara, *J. Mater. Chem. C*, 2014, **2**, 2674–2683.

27 S. Ji, T. Shi, X. Qiu, J. Zhang, G. Xu, C. Chen, Z. Jiang and C. Ye, *Sci. Rep.*, 2013, **3**, 2733.

28 K. Ramasamy, M. A. Malik and P. O'Brien, *Chem. Sci.*, 2011, **2**, 1170–1172.

29 M. R. Beaulieu, J. K. Baral, N. R. Hendricks, Y. Tang, A. L. Briseño and J. J. Watkins, *ACS Appl. Mater. Interfaces*, 2013, **5**, 13096–13103.

30 L. Huang, Z. Jia, I. Kymissis and S. O'Brien, *Adv. Funct. Mater.*, 2010, **20**, 554–560.

31 R. P. Ortiz, A. Facchetti and T. J. Marks, *Chem. Rev.*, 2010, **110**, 205–239.

32 N. A. Andrey and P. S. Igor, *J. Phys. D: Appl. Phys.*, 2010, **43**, 315104.

33 R. A. Picca, M. C. Sportelli, D. Hötger, K. Manoli, C. Kranz, B. Mizaikoff, L. Torsi and N. Cioffi, *Electrochim. Acta*, 2015, **178**, 45–54.

34 U. Bielecka, P. Lutsyk, K. Janus, M. Samoc, W. Bartkowiak and S. Nespurek, *Mater. Sci.-Pol.*, 2013, **31**, 288–297.

35 M. D. Heinemann, K. von Maydell, F. Zutz, J. Kolny-Olesiak, H. Borchert, I. Riedel and J. Parisi, *Adv. Funct. Mater.*, 2009, **19**, 3788–3795.

36 Z.-X. Xu, V. A. L. Roy, P. Stallinga, M. Muccini, S. Toffanin, H.-F. Xiang and C.-M. Che, *Appl. Phys. Lett.*, 2007, **90**, 223509.

This journal is © The Royal Society of Chemistry 2016

J. Mater. Chem. C, 2016, **4**, 5109–5115 | 5115